Chemical Engineering Journal 450 (2022) 138202

Contents lists available at ScienceDirect

Chemical Engineering Journal

journal homepage: www.elsevier.com/locate/cej

3D printed personalized, heparinized and biodegradable coronary artery stents for rabbit abdominal aorta implantation

Yihong Shen [a,1], Chaojie Tang [b,1], Binbin Sun [a], Yang Zhang [b], Xiaolin Sun [a], Mohamed EL-Newehy [c], Hany EL-Hamshary [c], Yosry Morsi [d], Hongbing Gu [e], Wu Wang [b,*], Xiumei Mo [a,*]

[a] State Key Laboratory for Modification of Chemical Fibers and Polymer Materials, Shanghai Engineering Research Center of Nano-Biomaterials and Regenerative Medicine, College of Biological Science and Medical Engineering, Donghua University, Shanghai 201620, PR China
[b] Institute of Diagnostic and Interventional Radiology, Shanghai Jiao Tong University Affiliated Sixth People's Hospital, Shanghai 200233, PR China
[c] Department of Chemistry, College of Science, King Saud University, P.O. Box 2455, Riyadh 11451, Saudi Arabia
[d] Faculty of Engineering and Industrial Sciences, Swinburne University of Technology, Boroondara, VIC 3122, Australia
[e] Department of Cardiovascular Surgery, Shanghai General Hospital, Shanghai Jiao Tong University School of Medicine, Shanghai 201600, PR China

ARTICLE INFO

Keywords:
Biodegradable coronary stents
3D printing
Personalized
Anti-coagulation
Abdominal aorta

ABSTRACT

Biodegradable stents have become the focus of attention in the field of interventional medicine. Compared to non-biodegradable stents, these stents are designed to degrade, leaving behind regenerating healthy arteries. In addition to biodegradability, customizability and anticoagulation are also important for stent treatments. The combination of magnetic resonance angiography (MRA) and 3D printing can customize coronary stents according to different vascular geometries of patients. Therefore, this work focused on the rapid fabrication of stents composed of polycaprolactone (PCL) by 3D printing and then functionalized the stents with heparin via covalent grafting. The 3D printed stents were implanted into the abdominal aorta of rabbits to evaluate the feasibility of implantation and biocompatibility. Mechanical tests showed that 3D printed stents have good mechanical properties. *In vitro* data demonstrated that the stents had excellent blood compatibility and cytocompatibility. The heparinized PCL(PCL-NH_2-Hep) stent can promote the adhesion, spreading and proliferation of human umbilical vein endothelial cells (HUVECs) and inhibit the excessive proliferation of smooth muscle cells (SMCs). Presently, there is insufficient study about 3D printed stent implantation in rabbit arteries. Hence, personalized stents were prepared via MRA and 3D printing, which tailored to the patient's unique anatomy. A 3D printed stent-balloon delivery system was employed to deliver stents to the abdominal aorta. At 3-month follow-up, the PCL-NH_2-Hep stent maintained good vascular patency. Moreover, the heparinized stents showed rapid endothelialization and prevention of neointimal restenosis *in vivo*. This study demonstrated that personalized PCL-NH_2-Hep stent may have the potential in the field of biodegradable coronary artery stents.

1. Introduction

Cardiovascular disease is one of the leading causes of global mortality, which is often related to vascular stenosis or occlusion[1]. Drug treatment is an effective way in the early stage of acute myocardial infarction[2]. When the effect of drugs on the disease is unsatisfactory, coronary artery stents need to be implanted in the diseased cardiac blood vessels to support the stenotic or occlusive vessels[3]. The coronary artery stents are usually made of metal and are permanent after implantation, which may cause the occurrence of the late stent thrombosis and very late stent thrombosis. In order to solve these problems, drug-eluting stents can be applied to reduce restenosis and thrombosis [4]. However, because of the nonbiodegradability, the drug eluting stents will remain in the body for a lifetime, preventing the complete recovery of vascular structure and function. It may also bring the risk of chronic inflammation, in-stent restenosis, and thrombosis due to its nondegradability of metals[5,6]. Therefore, it is necessary to develop a biodegradable coronary stent.

* Corresponding author.
E-mail addresses: wangwangwuwu@hotmail.com (W. Wang), xmm@dhu.edu.cn (X. Mo).
[1] These authors contributed to the work equally.

https://doi.org/10.1016/j.cej.2022.138202
Received 14 April 2022; Received in revised form 2 July 2022; Accepted 17 July 2022
Available online 21 July 2022

Recently, biodegradable stents have attracted wide attention in vascular repair and regeneration[7,8]. Biodegradable stent can maintain the role of supporting diseased blood vessels in the process of degradation. At the same time, it gradually degraded and finally degraded into small molecules, which allows the treated artery to regain its normal elasticity to dilate and contract. Braiding technique and laser engraving are widely used in the preparation of biodegradable stents[9]. Zhao et al., developed a PCL / poly (p-dioxane) (PPDO) stent with a diameter of 9 mm via braiding technique for congenital heart disease. They implanted stents into the abdominal aorta and iliac arteries of porcine. The stent could maintain target vessels with good patency in the follow-up[10]. Abbott has used extrusion and laser engraving techniques to fabricate Absorb BVS from poly-L-lactic acid (PLLA). Nevertheless, Absorb BVS has its drawbacks, such as poor anticoagulant activity, insufficient supporting force and uneven biodegradability, result in being removed from the market[11].

It is worth noting that both braiding technique and laser engraving have their own limitations[12]. The radial strength of braided stent structure is relatively insufficient, so it is difficult to meet the needs of long-term support in blood vessels[13]. Laser engraving may also cause thermal damage, which produce microcracks and stripes on the surface of the stent, leading to the fracture of the stent.[14]. In addition, the size range of stents made by braiding technique and laser engraving is very narrow, which further limits their applicability in vessels of different sizes. In recent years, 3D printing has received wide attention because of the characteristics of accurate rapid prototyping[15–17]. 3D printed stents can be customized according to the patient's specific lesion environment and vascular size. Compare to the rectangular strut of the laser-cutting stent, circular strut of 3D printed stent can reduce the interference of blood flow, which is more conducive to the recovery of normal endothelial function because of the smaller cross-sectional area [18].

Ideal biodegradable stent should not only have good mechanical properties, but also have the ability of anti-platelet deposition and anticoagulation[19]. At the same time, the stent can be individualized according to the patient's specific pathological environment and vascular dimension, and then accurately applied to vascular repair and treatment, so as to achieve the purpose of precision medicine.

The goal of this work is to develop a personalized biodegradable coronary artery stent that can be quickly prepared for clinical application. Due to the excellent biocompatibility, biodegradability, mechanical properties and processibility, PCL can be utilized in commercial 3D printers to print stents of different size for the requirement of coronary artery stents in interventional medicine[20]. For the preparation of personalized PCL stent, magnetic resonance angiography (MRA) can be used for angiography and 3D reconstruction of diseased blood vessels to determine the vascular size. After the stent model was designed and the stent size was determined by computer aided design, the computer model can be 3D printed with PCL to form customized biodegradable stents. In order to prevent post-implantation thrombosis, surface

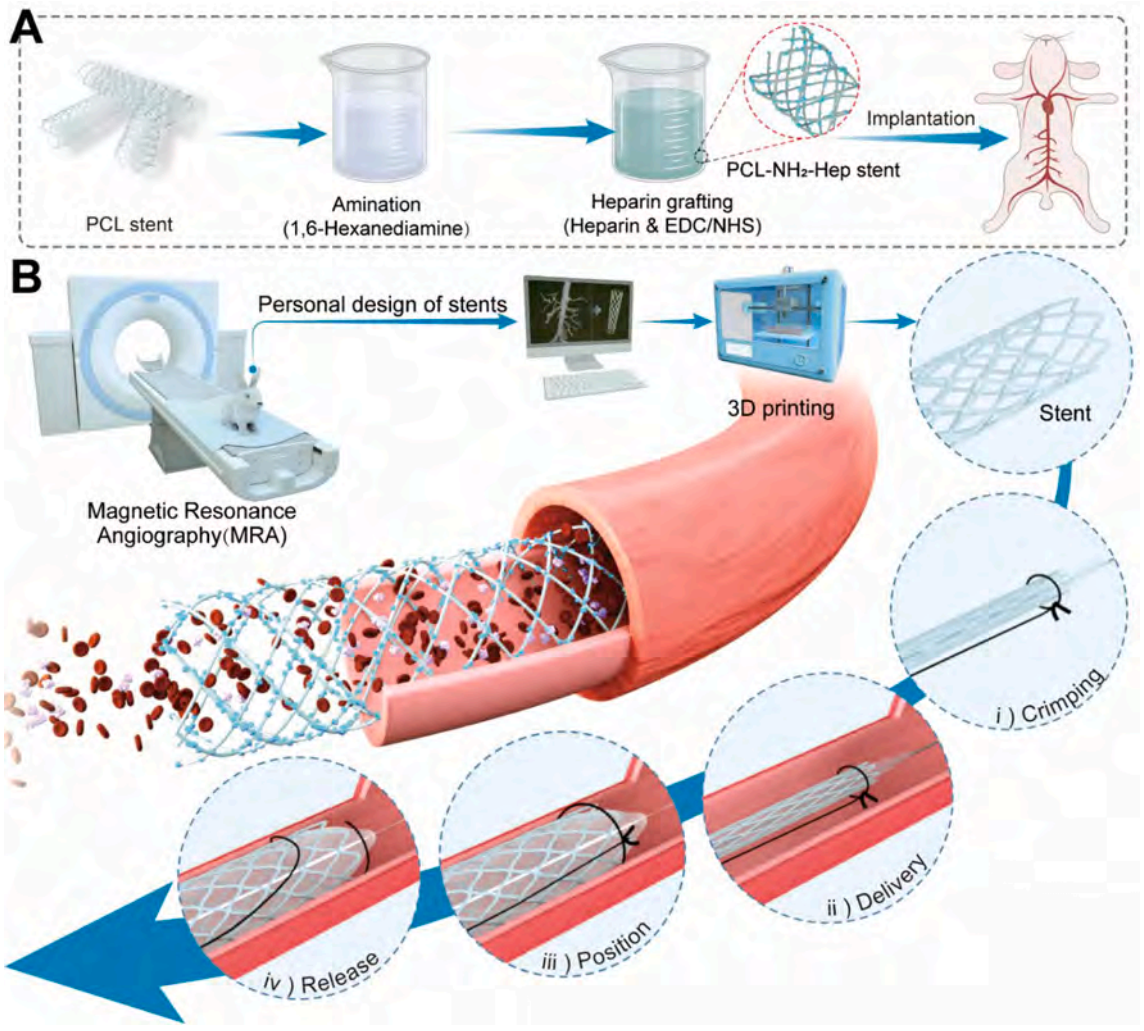

Fig. 1. (A) The process of heparinization modification of PCL stent. (B) Schematic illustration of 3D printing personalized, anticoagulant, and biodegradable coronary artery stents guided by magnetic resonance angiography (MRA).

modification of heparin was applied to 3D printed stents. As an acidic mucopolysaccharide, heparin has strong anticoagulant ability[21]. Previous studies have shown that heparin immobilized on the blood-contacting surface enhance the ability of anti-thrombosis *in vivo* [22,23].

In this work, we used 3D printing to prepare PCL coronary artery stents. Then, PCL stents were functionalized by covalent grafting with heparin to improve their anticoagulant ability (Fig. 1A). The biological properties of the stents were evaluated by cell culture *in vitro*. Subsequently, a stent-balloon delivery system was employed to deliver 3D printed stents to the rabbit abdominal aorta for observation of the feasibility of implantation and biocompatibility *in vivo* (Fig. 1B).

2. Materials and methods

2.1. Materials

Polycaprolactone (PCL) was purchased from Sigma-Aldrich ltd (St. Louis, USA). Heparin sodium was purchased from Beijing Labgic Technology ltd. CCK-8 was purchased by Beyotime Biotech Co., ltd (Shanghai, China). All culture medium and reagents were purchased from Gibco Life Technologies Co. (Carlsbad, California). All raw materials and reagents were used as received without purification.

2.2. Stent design and finite element analysis

Through theoretical calculation and analysis, the structural characteristic parameters of the stents were determined according to the following equation[24].

$$\text{Cross angle of interwoven fiber} = 2arctan\frac{30V_m}{R\cdot\pi R_r},$$

$$\text{Helix spacing} = \frac{60V_m}{R},$$

$$\text{Fiber parallel distance} = \frac{120\pi R_r\cdot V_m}{\sqrt[2]{4R^2\pi^2{R_r}^2+3600\cdot{V_m}^2}},$$

$$\text{Fiber diameter} = \frac{D_c\pm\sqrt{60V_c}}{\sqrt[4]{4R^2\pi^2{R_r}^2+3600\cdot{V_m}^2}}.$$

The parameters of 3D printing: D_e represents the inner diameter of the heating cavity for the printer, V_c represents extrusion rate, V_m represents nozzle print movement rate, R_r represents the radius of the rotating receiver, R represents the rotate speed of the receiver.

According to the above calculation formulas, the design of the stent and finite element analysis were carried out. The VonMise stress distribution of the stent model was obtained through the finite element analysis. The stent model and parallel plates were constructed by SolidWorks software (version 2019). Then the linear C3D4H (stent) and C3D8R (plate) element models were used to mesh in the ABAQUS software (version 2021). The interaction of two crossing fibers was set as a penalty function with a friction coefficient of 0.25. The two plates were fixed in all dimensions except the Y-axis displacement of the upper plate.

2.3. Fabrication of stents

2.3.1. Fabrication of 3D printing PCL stents

PCL was used as raw material for 3D printing. The PCL tubular stent was manufactured by 4-axis printing system, which consisted of a rapid prototyping manufacturing system (HTS-400; Fochif Mechatronics Technology, Co., China) and self-made rotary receiver. PCL was added to the extrusion chamber and preheat it to 120–130 °C for 20 min. The molten PCL was extruded through the nozzle at a temperature of 120–125 °C. The extrusion rate was 0.03 mm/min. The inner diameter of the extruder was 18 mm. The size of the nozzle was 22G. The extrusion nozzle moved at the speed of 1 mm/s along the central axis of the receiver. Stents of different sizes could be made from cylindrical receivers of different dimeters (2 mm-4 mm). The receiver rotated constantly at 15 revolutions per minute (n = 15). The printer kept reciprocating for 3 times. In addition, in order to complete the relevant characterization, the plate was used as the receiver to prepare planar stents.

2.3.2. Surface modification

2 g 1,6-Hexanediamine solid was added to 20 mL isopropanol solution. Subsequently, the PCL stent was added to 37 °C 20 mL 1–6-hexanediamine solution (0.1 g/mL) to treat for 1 h. Amino groups were formed on the surface of the PCL stent[25]. Aminated stents (PCL-NH_2) were prepared. After thoroughly washing the samples with deionized water, they were dried by vacuum dryer.

1 mg/mL heparin was dissolved in MES buffer (pH 5.5) containing 0.006 mol/L NHS and 0.012 mol/L EDC, and then the solution was kept at room temperature for 4 h to activate the carboxyl group of heparins. The aminated stents were immersed in activated heparin solution to shake at 37 °C for 24 h. The stents were cleaned with a large amount of deionized water to remove the by-products. After freeze-drying for 48 h, the heparinized PCL stents (PCL-NH_2-Hep) were obtained.

2.4. Fourier transform infrared spectroscopy (FTIR)

The chemical composition of the surface of PCL, PCL-NH_2 and PCL-NH_2-Hep stents was analyzed by the Fourier transform infrared spectrometer (ATR-FTIR, Nicolet 6700, USA). Diamond was used as the applied crystal, and 32 scans were performed with an absorption mode of 4 cm^{-1} over the range of 4000–400 cm^{-1}.

2.5. Scanning electron microscopy (SEM)

The morphology and microstructure of PCL, PCL-NH_2 and PCL-NH_2-Hep stents were observed by scanning electron microscope (SEM, PhenomXL, Netherlands). Before observation, SEM samples were sputter coated with gold–palladium by a mini sputter coater (SC7620, Quorum Technologies, USA). The current was set to 12 mA, the vacuum chamber pressure was set to approximately 6×10^{-2} mbar, and time was set to 60 s. Then stents were characterized by scanning electron microscope under the accelerated voltage of 10 kV.

2.6. Water contact angle

The apparent water contact angle of PCL, PCL-NH_2 and PCL-NH_2-Hep stents was measured three times using a contact angle instrument (OCA40, Data-Physical, Germany). 0.05 mL distilled water was slowly dripped to the surface of the sample. After the water droplets remained stable, the camera software in the test system was utilized to record the image of the water droplets on the sample.

2.7. In vitro release behavior of heparin

To confirm the heparin's stability of PCL-NH_2-Hep stents, each testing sample of was immersed in phosphate buffer saline (PBS) solutions (pH 7.4). Afterward, the testing samples were shaken continuously on a horizontal shaker at 37 °C and 100 rpm. At the predetermined time point, the testing samples were retrieved. Then toluidine blue assay was adopted to measure the content of heparin in the released solution. All testing samples were measured and analyzed for three times.

2.8. Energy dispersive spectrum

The distribution of elements (C, O and S) on PCL-NH_2-Hep stent was measured by Energy Dispersive Spectrometer (EDS, TM-1000, Hitachi, Japan).

2.9. Mechanical properties

According to ISO25539-2012 (standard), the compression performance of the stent was tested by a universal testing machine (HY-940FS, Shanghai Hengyu Instrument Co., ltd, China) with a 20 N sensor. PCL, PCL-NH_2 and PCL-NH_2-Hep stents were compressed to 50 % of their outer diameter, then hold for 30 s. The compression load–displacement

curve was obtained by reading and calculating the corresponding compression force. Each stent was compressed to a strain of 50 % for 10 cycles at a rate of 5 mm/min in compressive and fatigue test. Compression cycle curve of stent was obtained. The three-point bending test was carried out according to ASTM F2606-09 (standard), the standard guide for three-point bending of balloon expandable coronary artery stents and stent systems. The length of the stent was set to 10 mm. The maximum displacement of the pressure device was 1.75 mm, and the displacement rate was 0.1 mm/min.

2.10. Evaluation of blood compatibility

Hemolysis rate: hemolysis test was carried out *in vitro* with 2 % (v/v) erythrocyte suspension. The fresh whole blood of New Zealand rabbits was centrifuged by 3000 rpm for 10 min. The obtained erythrocyte suspension was washed with normal saline for three times, followed by further diluting to a suspension with a final concentration of 2 % (v/v). Each testing sample was preheated for 30 min in 37 °C 10 mL saline. 0.2 mL 2 % (v/v) erythrocyte suspension was dropped into the above testing sample, and then gently mixed. After incubation at 37 °C for 1 h, all the mixtures were centrifuged under 3000 rpm to precipitate intact erythrocyte. The supernatant was carefully transferred to a 96-well plate and measured the absorbance at 540 nm. 0.9 % normal saline (NS) was set as negative control and deionized water as positive control.

Platelet adhesion: Platelet-rich plasma (PRP) was prepared from whole blood after centrifugation to obtain the PRP supernatant. The testing samples were incubated with 500 μL PRP at 37 °C for 2 h. After incubation, platelets were fixed to the samples. Then the testing samples were washed with warm PBS solution to remove un-adherent platelets on the surface of the stent. The testing sample was then fixed with paraformaldehyde for 2 h. The testing samples were rinsed with distilled water twice. A series of graded ethanol solutions (30, 50, 70, 80, 90, and 100 %) was used to dehydrate the testing samples and then freeze-dried. Finally, samples were sputter coated with gold–palladium, and the morphology of adherent platelets was observed by SEM.

The anticoagulant ability of the stent was evaluated by activated partial thromboplastin time (APTT) and prothrombin time (PT). Platelet-poor plasma (PPP) was prepared from whole blood after centrifugation to obtain the PPP supernatant. Stents with length of 10 mm and diameter of 3.5 mm were used to incubate in 100 μL PPP at 37 °C for 2 min. In prothrombin time test, PT reagent (100 μL) was added to the incubated sample, and the prothrombin time was recorded. In activated partial thromboplastin time test, above samples were incubated in 100 μL APTT at 37 °C, and then 0.025 μmol/L $CaCl_2$ solution (100 μL) was added into above samples. The activated partial thromboplastin time was recorded[26].

2.11. Cytocompatibility assay

For the evaluation of cell viability, the planar stents (14 mm × 14 mm) were used. For this study, the planar PCL, PCL-NH_2 and PCL-NH_2-Hep stent samples were secured in 24-well plates by stainless steel rings. Before cell seeding, all samples were irradiated with UV light for 12 h after sterilizing with 75 vol% alcohol steam for 24 h. The distance between light and samples was set as 20 cm. After sterilization, the samples were washed with PBS for three times. The cell culture medium (300 μL) was added to each well. Then the testing samples were incubated at 37 ℃ for 4 h in an atmosphere containing 5 % CO_2. HUVECs were seeded on the samples at a density of 3×10^4 cells per well and additional 200 μL cell culture medium was added. After 1, 4 and 7 days of culture, DMEM containing 10 % CCK-8 reagent was used instead of cell culture medium to detect the proliferation of HUVECs. After two hours, 100 μL of the solution was pipetted into a 96-well plate, and the absorbance at 450 nm was measured using a microplate reader (Multiskan MK3, Thermo, USA).

In addition, the samples were placed in a 24-well culture plate and incubated with 300 μL cell culture medium at 37 ℃ for 4 h. HUVECs were seeded on the samples at a density of 3×10^4 cells per well and additional 200 μL cell culture medium were added. After 4 or 7 days of cultivation, the cells were stained using a live cell staining kit (Beyotime, China), in accordance with the manufacturer's instructions. Living cells were observed using a fluorescent microscope (DMi8, Leica, Germany). The sample was then fixed with paraformaldehyde for hours. The fixed samples were dehydrated through a series of graded ethanol solution after rinsing with distilled water and then freeze-dried. Finally, samples were sputter coated with gold–palladium, and the morphology of HUVECs was observed by SEM.

With the same process, 3×10^4 human vascular smooth muscle cells per hole were seeded on the stent. The proliferation of SMCs on the surface of PCL, PCL-NH_2 and PCL-NH_2-Hep stent samples was evaluated. At the same time, fluorescence microscopic morphology and SEM images of SMCs on the surface of stents after 4 and 7 days were also observed.

2.12. In vitro degradation of the stents

PCL, PCL-NH_2 and PCL-NH_2-Hep stents were immersed into 10 mL PBS (pH 7.4). Afterward, the testing samples were shaken continuously on a horizontal shaker at 37 °C and 100 rpm. At the expected point of time, testing samples were retrieved. After rinsing with distilled water, the remaining buffer salt on the testing samples was removed. The samples were then freeze-dried. The morphology and the mechanical property of the stents were assessed. All testing samples were measured and analyzed for three times.

2.13. In vivo assessments

More than 20 New Zealand white rabbits (weight 2.5–3.3 kg, 5–8 months old) were selected for PCL, PCL-NH_2 and PCL-NH_2-Hep stent implantation. After 30 min of ultraviolet sterilization, a stent (size: 3.5 × 15 mm) was pressed into 5.5-F catheter guide sheath in advance. Then rabbits were anesthetized with a single administration of an intramuscular injection of xylazine at 0.1 mg/kg and 1 % sodium pentobarbital at 1 mg/kg. Animals were breathing spontaneously during surgery. For each of the rabbits, the right groin skin was shaved, sterilized and an incision was made in the angiographic unit. Subsequently, exposed and punctured the femoral artery for placing a 6-F catheter sheath into the artery. A 6-F guiding catheter was advanced into the proximal segment of abdominal aorta. The angiography showed the patency of abdominal aorta. The biodegradable suture (5–0 Coated VICRYL, Cordis, US) was knotted in the same direction (temporary knot) to fix the 3D printed stent on the high compliance balloon (Emerge Monorail, Boston Scientific, US). The entire device was named 3D printed stent -balloon system. The suture was also fixed to the catheter near the balloon with a surgical knot. The 3D printed stent-balloon system was advanced with the microguide wire guiding into the 6-F guiding catheter via the catheter guide sheath, and finally into the middle segment of abdominal aorta under roadmap. After angiography showed the right location of the 3D printed stent-balloon system, the balloon was dilated with a pressure pump to release the stent, and the temporary knot was opened while the pressure over 8 kPa. The stent was usually implanted into the distal segment of the abdominal aorta (2–3 vertebral segments below the renal arteries). Angiography was performed to show the condition of stent and the patency of abdominal aorta. Finally, the system was pulled back. The last step was to close the wound of the right groin in multiple layers with 3–0 Vicryl. This procedure lasted for approximately-one hour. All rabbits were fed with adequate water and food in cages after the operation and then intravenously injected with heparin (400 U) for three days. All animals were also administered aspirin (10 mg) and clopidogrel (7.5 mg) 1 day before the procedure and up to termination.

To detect vessel patency of rabbits which received stent implantation, Digital Subtraction Angiography (DSA) was performed at 2, 4 and

12 weeks after implantation. At predetermined time points, rabbits were sacrificed by injecting an over-dose of isoprene barbiturate. The arteries contained the stents of the rabbits were retrieved. The re-endothelialization of the implanted stent was observed by SEM, and the tissue regeneration was detected by Hematoxylin and eosin staining (H&E), immunofluorescence staining and immunohistochemical staining. Neointimal area, neointimal stenosis rate and inflammatory cell numbers in the neointima were measured according to H&E staining.

2.14. Statistical analysis

Statistical data was expressed as the mean ± standard deviation (SD). The analysis of data was performed using a one-way ANOVA, followed by Tukey's post hoc test. * Indicates significant difference of $p < 0.05$. # Indicates no significant difference of $p > 0.05$.

3. Results

3.1. Finite element analysis

Finite element analysis is an effective way to optimize the structure design of vascular stents. The structure of the stent was shown in Fig. 2A. The stent was composed of well-organized fibers. Fiber was firmly combined in the upper and lower layers to form a stable stent structure. The intersection of the two filaments was bonded together to make the stent have better mechanical resistance under the external force. The compression and tension performance of the stent could be simulated by using the established stent model for three-dimensional finite element analysis. The VonMise stress distributions under compression and tension were shown in Fig. 2B. The compression deformation of PCL stent was mainly concentrated at the intersection. The stress distribution of the stent strut was relatively uniform. The stress concentration zone appeared near the bonding point. The designed stent could maintain a stable shape under a compression strain of up to 50 %. It could help maintain vascular support and better compression resistance during vasodilation and contraction. At the same time, the structural integrity changes pre-operation and post-operation may potentially develop into the fracture of stents after implantation. Tensile property is essential for 3D printed stent crimping. In the process of tension, the maximum stress of the stent was mainly concentrated in the center of the inner surface of the strut, but the stress distribution was still relatively uniform. The low stress concentration reduced the potential damage caused by deformation, which was beneficial to the crimp of stent and delivery of the 3D printed-stent-balloon system.

3.2. Characterization of stent

We used biodegradable PCL and processed it into tubular stents via 3D printing and then functionalized the stents with heparin via step-by-step covalent grafting. PCL was heated to melt to extrude from the 3D printer. Through the reciprocating movement of the printer, the PCL fibers could be collected by different diameters of stainless-steel rod (Fig. 3A). The stents could maintain tubular shape after removed from the stainless-steel rod and stents of different sizes can be prepared (Fig. 3B). 1,6-Hexanediamine solution has been widely utilized in order to introduce amino group into polyester materials[27,28]. In order to functionalize the PCL stent, $–NH_2$ functional groups were introduced on its surface by 1,6-Hexanediamine treating. The aminated PCL stent was stained purplish red after Ninhydrin hydrate staining (Fig. 3C). The presence of $–NH_2$ groups could be confirmed. Then EDC-NHS was used to realize the coupling between the carboxyl group of heparins and the amino group of PCL-NH_2, thus realizing the covalent grafting of heparin. After toluidine blue staining, the heparinized stent exhibited blue-purple color, which verified the presence of assembled heparin (Fig. 3D). As shown in Fig. 3E, the characteristic absorption peaks of PCL stent were at 1720 cm^{-1}(C═O carbonyl stretching) and 1170 cm^{-1}(C—O—C

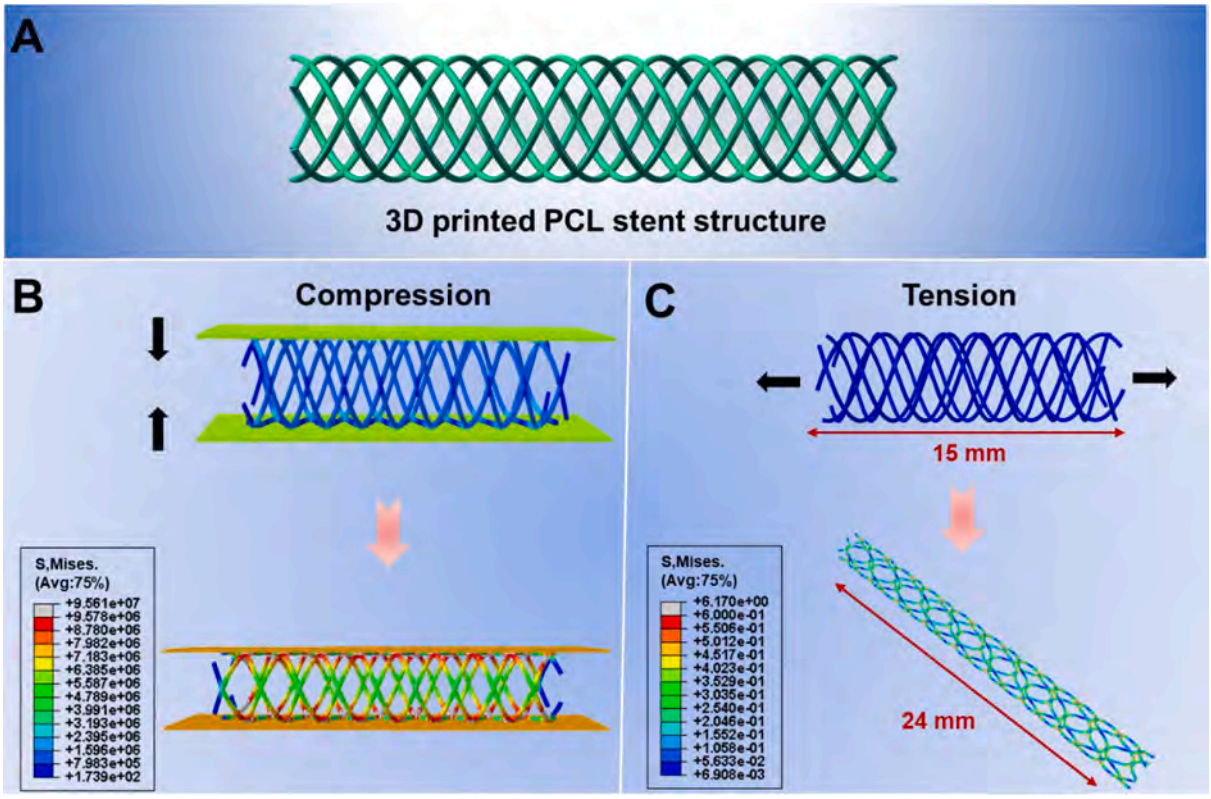

Fig. 2. (A) Scheme of the 3D printed stent structure. Finite-element analysis results for the Von Mise stress distribution of stents under parallel compression (B) and tension (C).

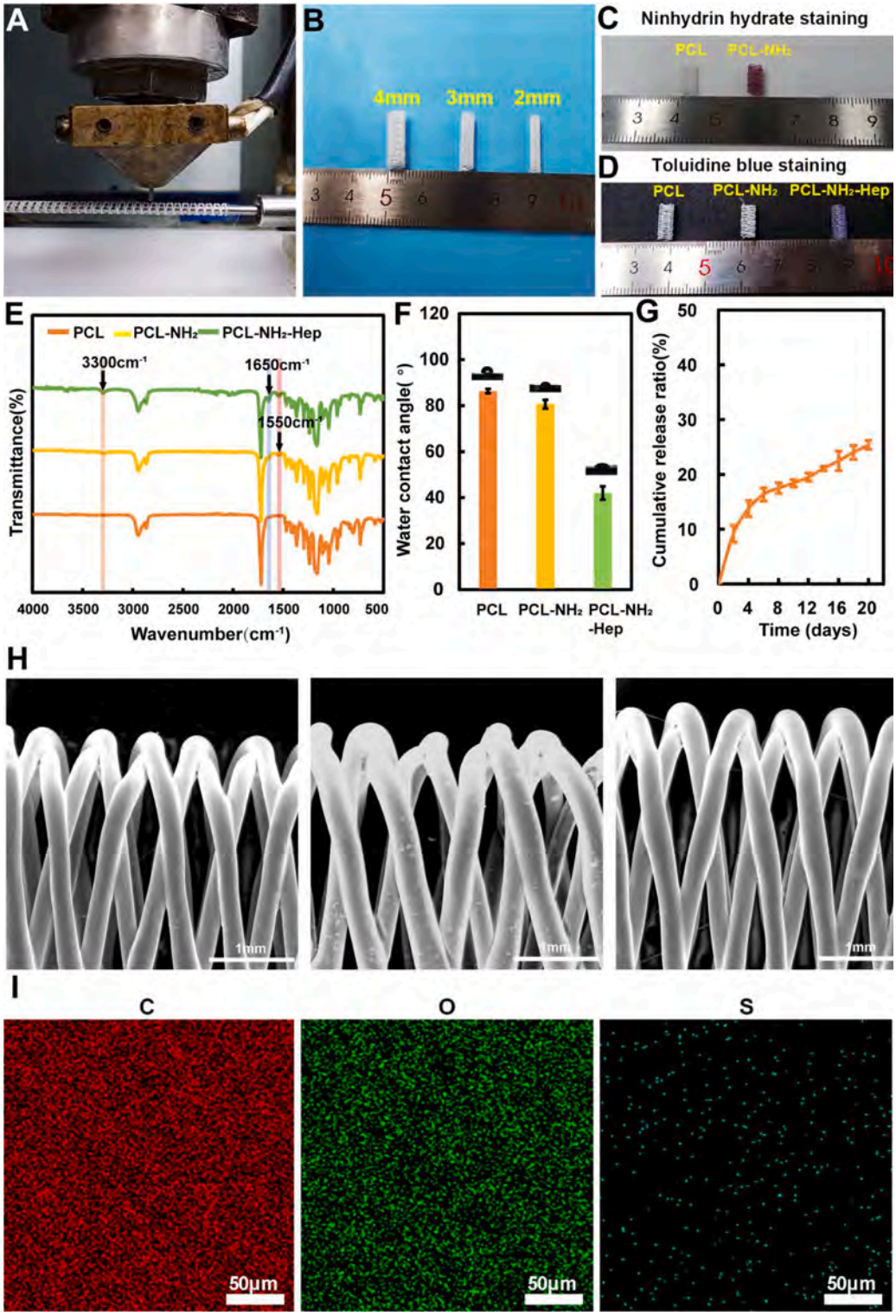

Fig. 3. (A) Fabrication and construction of stents via 3D printing. (B) Digital photos of various sizes of PCL stents. (C) Outer surface of the stent after Ninhydrin staining (PCL, PCL-NH_2). (D) Outer surface of the stent after Toluidine blue staining (PCL, PCL-NH_2, PCL-NH_2-Hep). The FTIR spectra (E) and water contact angles (F) of PCL, PCL-NH_2 and PCL-NH_2-Hep stents. (G) The release profile of heparin from PCL-NH_2-Hep stents for 20 days (H) SEM micrographs of stents. (I) The EDS element mapping of PCL-NH_2-Hep stent.

stretching vibration). A new peak of 3300 cm^{-1}(N—N amine stretching) and 1550 cm^{-1}(N—H amide bending) appeared on PCL-NH_2 stent after amination, which indicated that the amination process had been completed. After heparin functionalization, PCL-NH_2-Hep had obvious characteristic peaks in FTIR spectra. The characteristic peaks of heparin were observed at 1650 cm^{-1} (protonated amine vibration). The N—H stretching vibrations (3300–3400 cm^{-1}) was further increased on PCL-NH_2-Hep stent compared to PCL-NH_2 stent. It was confirmed that heparin was successfully grafted on the surface of PCL stents[29].

In views of SEM images, the stent was made of well-organized fibers. The staggered fiber surface was smooth and the intersection point was uniform. There was no significant difference in the surface of PCL modified by ammonolysis and immobilized with heparin (Fig. 3H). The surface hydrophilicity was determined by contact angle test (Fig. 3F). The PCL stent showed hydrophobicity, and the contact angle was 86°. After amination, the hydrophilicity was slightly improved, and the contact angle was 83°. The surface of PCL-NH_2-Hep stent was hydrophilic after covalent modified with heparin because of a large number of

polar groups from heparin, such as carboxyl and sulfate groups. After the grafting of heparin, the contact angle decreased to 42°. Moreover, the heparin release ratio was shown to confirm the heparin's stability of PCL-NH_2-Hep stents in Fig. 3G. After immersion in PBS for 20 days, 25.4 % of heparin had released. No burst release was observed, indicating the excellent stability of heparin modified surface. The covalent bonds between PCL and heparin ensured the stability of the heparin.

The EDS element mapping (Fig. 3I) illustrated the distribution and density of carbon, oxygen and sulfur in the stent. Theoretically, in our system, sulfur was the characteristic element of heparin. EDS element mapping showed that sulfur was evenly distributed in PCL-NH_2-Hep stents.

3.3. Mechanical properties

Mechanical property is essential for stent implantation and intravascular support. Compression performance, including compression force and stress relaxation, is a major challenge for polymeric stents. The radial compression performance of the stent was shown in Fig. 4A. The compression modulus of PCL stent was 2086.63 ± 117.58 mN/mm. The compression modulus was 2030.9 ± 182.35 mN/mm and 1980.67 ± 83.68 mN/mm after amination and heparinization respectively. Fig. 4B presented the results of compressive force. The compression force of PCL stent was 308.2 cN. The compression force was 327.3 cN and 312.5 cN after amination and heparinization respectively. As shown in Fig. 4C, the average stress relaxation of the PCL group was 0.45 ± 0.04 N. After amination and heparinization, it was increased to 0.46 ± 0.04 N (PCL-NH_2 group) and 0.49 ± 0.11 N (PCL-NH_2-Hep group), respectively. It was indicated that the compression modulus, compression force and stress relaxation behavior would not change with the surface modification of the stent. The ten times cyclic compression test (Fig. 4E) ensured the stability of the PCL, PCL-NH_2 and PCL-NH_2-Hep stents.

According to the standard guidelines for three-point bending test of ASTM F2606-09 vascular stents, three-point bending tests of PCL, PCL-NH_2 and PCL-NH_2-Hep stents were carried out. As shown in Fig. 4D, all the stents were bendable and returned to their original shape, with no

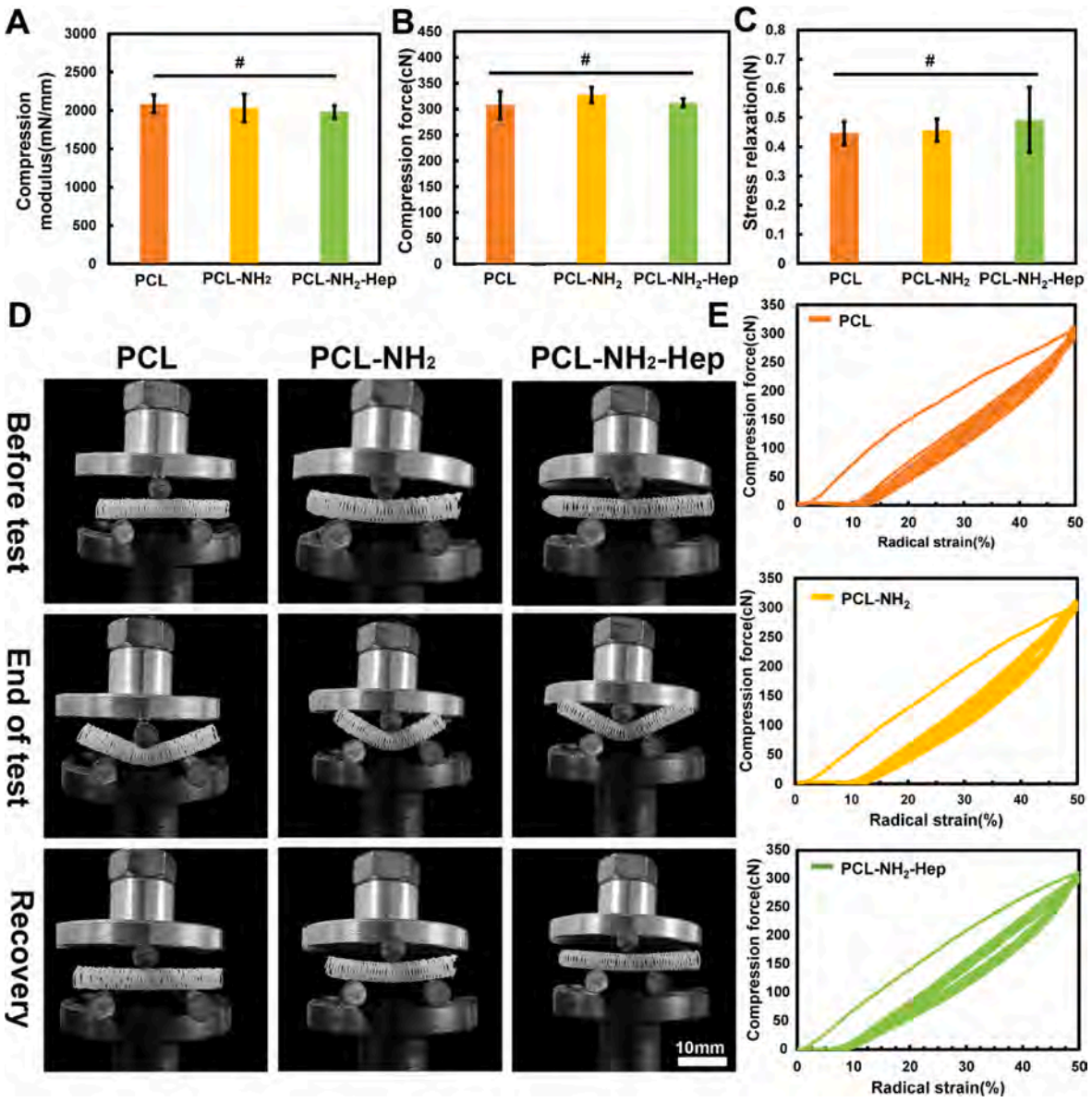

Fig. 4. *In vitro* mechanical properties. (A) Compression modulus, (B) Compression force and (C) Stress relaxation of PCL, PCL-NH_2 and PCL-NH_2-Hep stents, when radially compressed to half the initial diameters. (D) Images of three-point bending tests. (E) Typical compression load–displacement curves of stents when they were cyclically compressed for ten times. (*Indicates significant difference of $p < 0.05$. # Indicates no significant difference of $p > 0.05$).

obvious signs of damage or permanent deformation. The stent had good bending resistance, which is the key characteristic of catheter-assisted stent implantation. To sum up, these results showed that the 3D printed stent had good mechanical properties and could provide the necessary intravascular support for surgical implantation.

3.4. In vitro degradation of the stent

Fig. 5A showed a representative SEM image of the PCL, PCL-NH_2 and PCL-NH_2-Hep stents after 15, 30, 45 and 60 days of degradation in PBS solution. It is noteworthy that the surface morphology of the stent had not changed significantly after the one-month degradation periods. The overall structure was still intact. After degradation for 60 days, slight cracks appeared on the surface of the fiber, but the structure remained unchanged and stable. During the 60 days degradation, all stent struts and cross-points remained stable. Fig. 5B, 5C, 5D showed that there was no significant change in the mechanical properties of the stent.

3.5. Blood compatibility and inhibition of platelet adhesion

According to ISO10993-4 (standard), hemolysis test was conducted to evaluate the blood compatibility of stents [30,31]. The PCL-based stent showed good blood compatibility, as shown in Fig. 6A. Both the unmodified and surface-modified stents had hemolysis rates of about 0.5 %, indicating that the covalent graft of heparin did not affect the hemolysis characteristics of the stents. Under ISO10993-4 standards for blood-contacting materials (5 %), these stents could be considered non-hemolytic and may be safe for implantation.

When the allogeneic material comes into contact with blood, fibrin in blood is easily adsorbed on the surface of the material, leading to a chain reaction: platelet adhesion, activation, aggregation and finally thrombosis. A typical SEM image of platelet adhesion on PCL-based stents after 2 h incubation of PRP was shown in Fig. 6B. The SEM images showed that platelets were evenly adhered to the surface of the PCL-based stents, but no platelet aggregation was observed. Compared with PCL, the aminated stents showed more platelet adhesion. However, heparin covalently modified stents had less platelet deposition and would not cause platelet deformation. The results showed that covalently modified heparin stents had anticoagulant activity and might be able to prevent intravascular coagulation.

PT and APTT tests were used to evaluate the effects of materials on intrinsic and extrinsic coagulation pathways, respectively. The PT values of PCL-NH_2-Hep group (29.5 ± 2.0 s) were significantly higher than those of PCL-NH_2 group (12.4 ± 1.8 s) and PCL group (10.7 ± 0.4 s) (Fig. 6C). Similarly, The APTT values of PCL-NH_2-Hep group (86.3 ± 4.8 s) were significantly higher than those of PCL-NH_2 group (36 ± 2.2 s) and PCL group (38.3 ± 2.6 s) (Fig. 6D). Therefore, heparinized stents can inhibit the activation of intrinsic and extrinsic coagulation pathways and inhibit the development of thrombus.

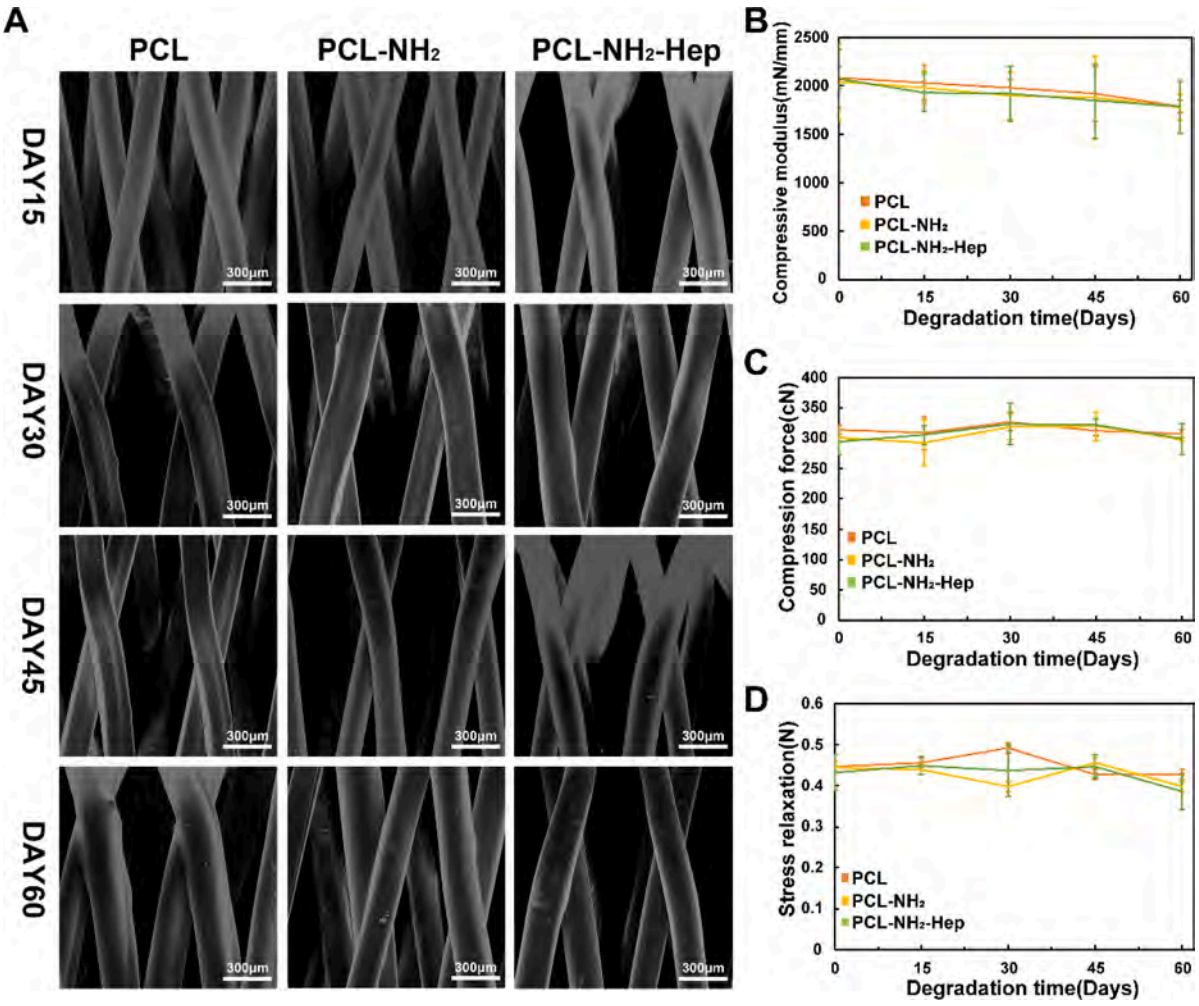

Fig. 5. Degradation evaluation of stent *in vitro* environment. (A) Representative SEM micrographs of stents during 60 days degradation. (B) Compression modulus, (C) Compression force and (D) Stress relaxation of PCL, PCL-NH_2 and PCL-NH_2-Hep stents during 60 days degradation.

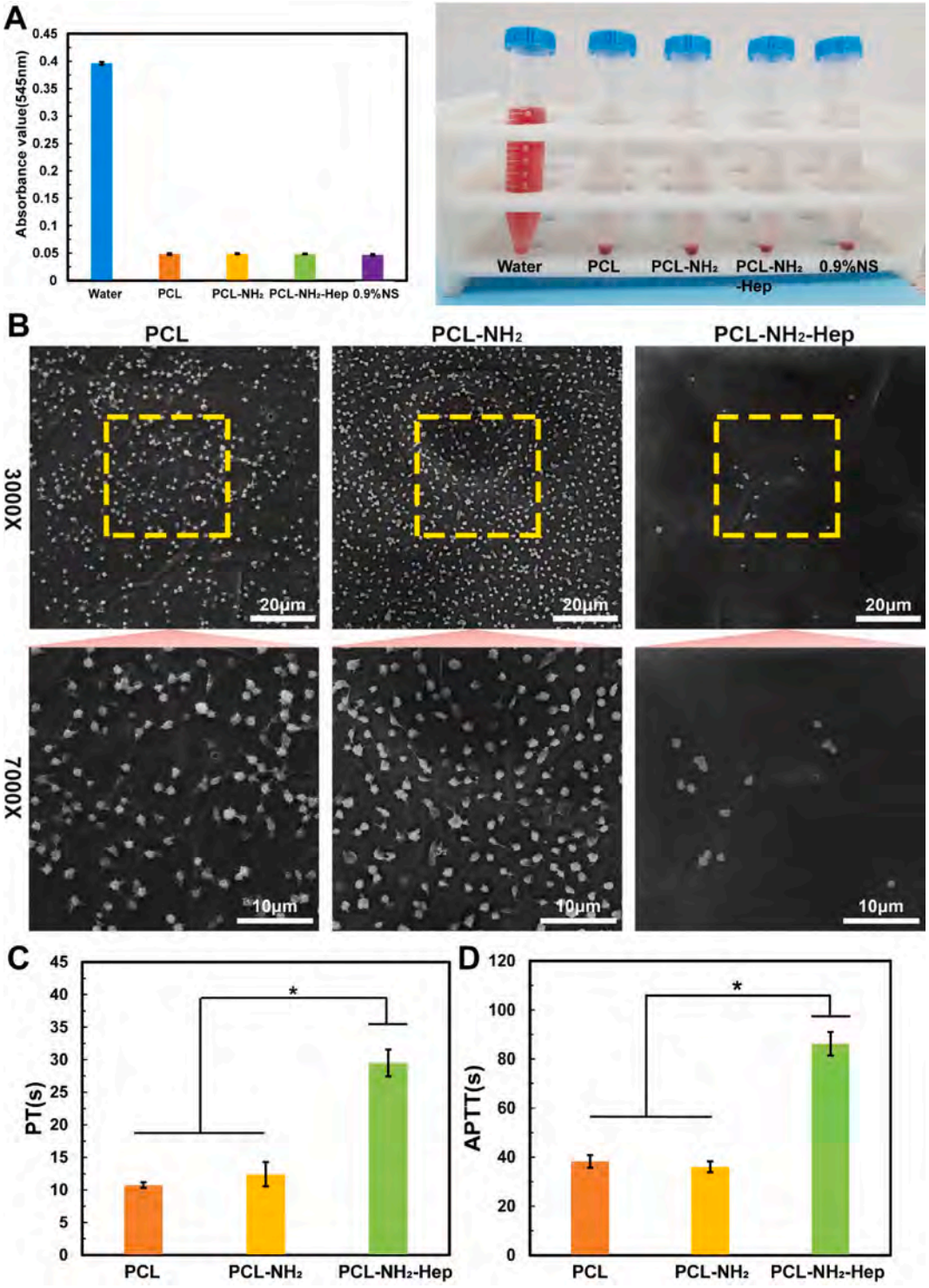

Fig. 6. Blood compatibility of stents. (A) Quantification and digital photos of relative hemolysis rate. (B) Platelet adhesion determined by SEM images. Coagulation time of PT (C) and APTT (D). (*Indicates significant difference of $p < 0.05$. # Indicates no significant difference of $p > 0.05$).

3.6. Behavior of HUVECs on stents

It is essential to form the healthy endothelial layers on the surface of the stent for the prevention of late stent restenosis and late stent thrombosis [32]. HUVECs were seeded on the surface of the stents to observe the ability of the stents to regenerate rapid endothelium formation. The proliferation (Fig. 7A) and adhesion (Fig. 7B) of HUVECs on 3D printed stents were evaluated. In the process of 7 days of cell culture, the absorbance of CCK-8 in each group increased steadily, indicating that all the testing samples supported HUVECs growth. Both modified and unmodified stents support the adhesion and proliferation of HUVECs and have good cell compatibility. After 1 day culture, there was no significant difference in the number of HUVECs between the samples. The number of HUVECs on the PCL-NH_2-Hep stent was significantly higher than that on PCL and PCL-NH_2 stent after 4 days and 7 days culture (Fig. 7A). In addition, HUVECs were observed on Calcein-AM stained samples after 4 and 7 days of culture (Fig. 7B). The results showed that the cells showed good morphology on the surface of the

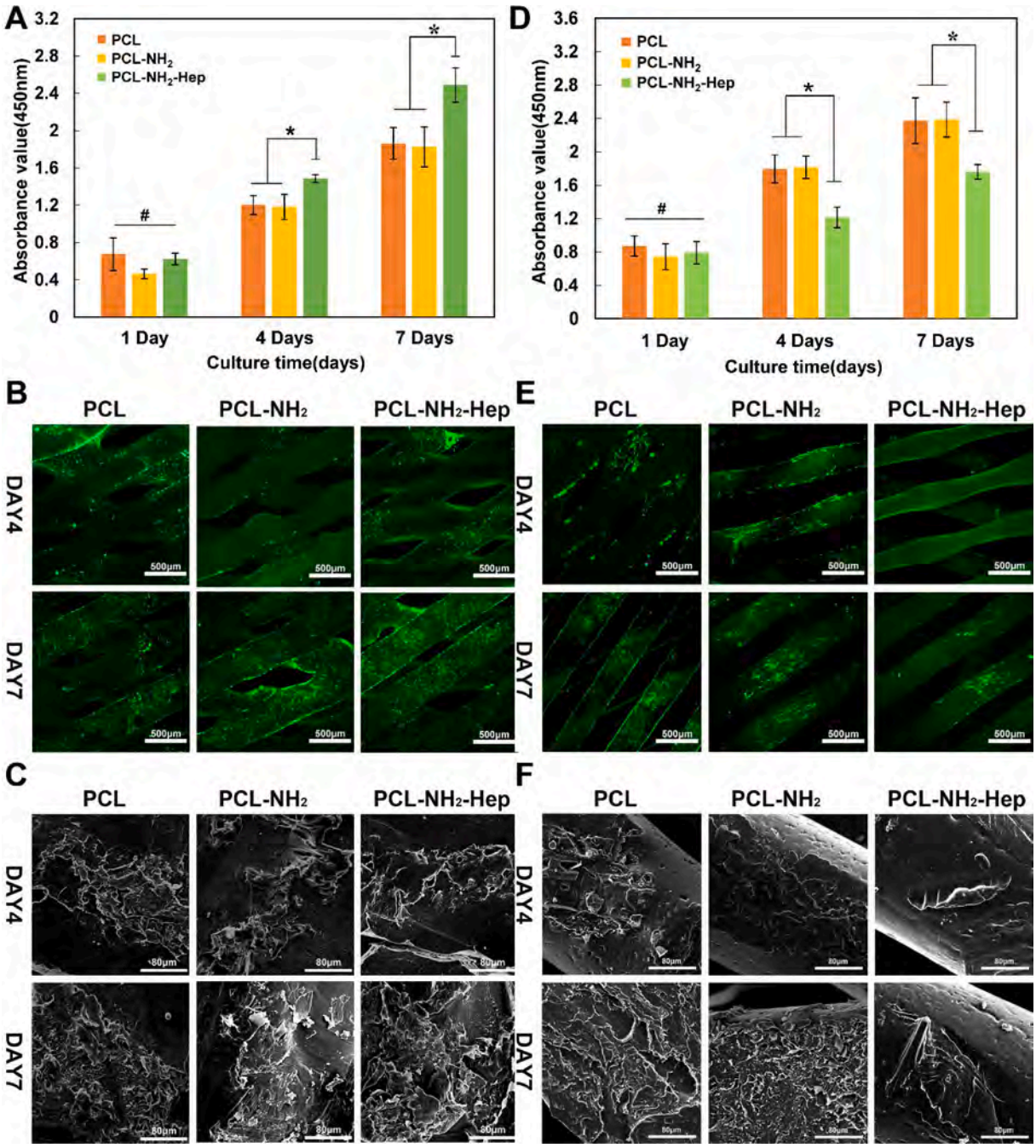

Fig. 7. (A) Proliferation of HUVECs on the surface of stents. (B) Fluorescence microscopic morphology of HUVECs cultured on the surface of stents after 4 and 7 days. (C) SEM images of HUVECs cultured on stents after 4 and 7 days. (D) Proliferation of SMCs on the surface of stents. (E) Fluorescence microscopic morphology of SMCs cultured on the surface of stents after 4 and 7 days. (F) SEM images of SMCs cultured on stents after 4 and 7 days. (*Indicates significant difference of $p < 0.05$. # Indicates no significant difference of $p > 0.05$).

stent struts at time points of 4 days. After 7 days of culture, more HUVECs were observed on PCL-NH_2-Hep stent than on PCL and PCL-NH_2 stent.

The morphology of the HUVECs on the surface of the stent was observed by SEM (Fig. 7C). After 4 days culture, cells began to proliferate in each sample, and numerous clumps of adherent cells were found on the surface of PCL-NH_2-Hep stents. At Day 7, the luminal surface of each sample showed significant cellular coverage. PCL-NH_2-Hep stents positively influenced the HUVECs attachment and proliferation. Morphological analysis showed that the cells attached and elongated on the PCL-NH_2-Hep stent. Heparinized samples were more suitable for the proliferation of HUVECs, because the heparin enhanced the adhesion of HUVECs.

3.7. Behavior of SMCs on stents

Intimal hyperplasia caused by overproliferated SMCs is a major factor in luminal stenosis and thrombosis[33]. SMCs were seeded on the surface of stents to evaluate the effect of SMCs growth on different stents *in vitro*. The proliferation (Fig. 7D) and adhesion (Fig. 7E) of SMCs on 3D printed stents were evaluated. After 1 day of culture, there was no significant difference in the number of SMCs between samples. The number of SMCs adhered to PCL-NH_2-Hep stents was significantly less than that of PCL-NH_2 and PCL stents after 4 days and 7 days culture, which

showed that the introduction of heparin inhibited the proliferation of SMCs. In addition, SMCs were observed on Calcein-AM stained samples after 4 and 7 days of culture (Fig. 7E). The results showed that the proliferation rate of SMCs in PCL-NH_2-Hep group decreased at Day 4. After 7 days of culture, the adhesion of SMCs on the surface of PCL-NH_2-Hep stent was less than that of PCL and PCL-NH_2 stents, indicating that the heparinized stent inhibited the proliferation and adhesion of SMCs, which was consistent with the experimental results of CCK-8.

The morphology of the SMCs on the surface of the stent was observed by SEM (Fig. 7F). At time points of 7 days, the cells spread well on PCL and PCL-NH_2 group and adhered to many cell clusters. However, the adhesion on PCL-NH_2-Hep was inhibited. After 7 days of culture, the luminal surface of PCL and PCL-NH_2 showed significant cellular coverage, but continuous cell layer could not form on PCL-NH_2-Hep stent. This suggests that heparin inhibits SMCs proliferation.

3.8. *In vivo examination*

MRA images (Fig. 8A) were used to determine the diameter of the stent for *in vivo* study. The success of the surgery demonstrated the feasibility of this method for vascular measurement and stent implantation. We prepared 3D printed stents based on their dimensions and functionalized them with heparin via covalent grafting, followed by implanting PCL-NH_2-Hep stent and the control stents (PCL stent and PCL-NH_2 stent) into the abdominal aorta of rabbits. Before the implantation of the stent, the biodegradable suture was knotted in the same direction (temporary knot) to fix the stent on the high compliance balloon. The suture was also fixed to the catheter near the balloon with a surgical knot. The 3D printed stent-balloon system was advanced with the micro-guide wire guiding into the 6-F guiding catheter via the catheter guide sheath. After the 3D printed stent-balloon system was in the correct position, the balloon was expanded to release the stent (Fig. 8B).

Fig. 8C showed angiography images of the stent status taken after 2, 4 and 12 weeks post-implantation. Angiography images showed that stents were implanted successfully in all cases, with no signs of intraluminal defects. The angiograms revealed that all stents were patent 90 days after surgery. Images can validate the patency of PCL and PCL-NH_2-Hep stented vessel, but severe stenosis occurred in PCL-NH_2 group.

A healthy, intact endothelium can protect blood vessel intima from blood clots, inflammation, and arteriosclerosis. All groups of stents were retrieved 2, 4 and 12 weeks after surgery for overall assess. SEM was used to visualize the endothelial coverage and platelet adhesion. Fig. 8D showed that endothelial cells layers were homogeneously covered on the surface of the PCL-NH_2-Hep stents after 30 days. At 12 weeks, endothelial cells were well organized align to the direction of blood flow. No thrombus matrix or platelet adhesion was observed in the lumen of the PCL-NH_2-Hep group, indicating that it has great capacity of antithrombosis. However, incomplete reendothelialization and a large number of platelets were observed on PCL-NH_2 group.

H&E staining (Fig. 9A) showed that the stent gradually began to form new tissue in the vascular lumen after 2 weeks of implantation, and

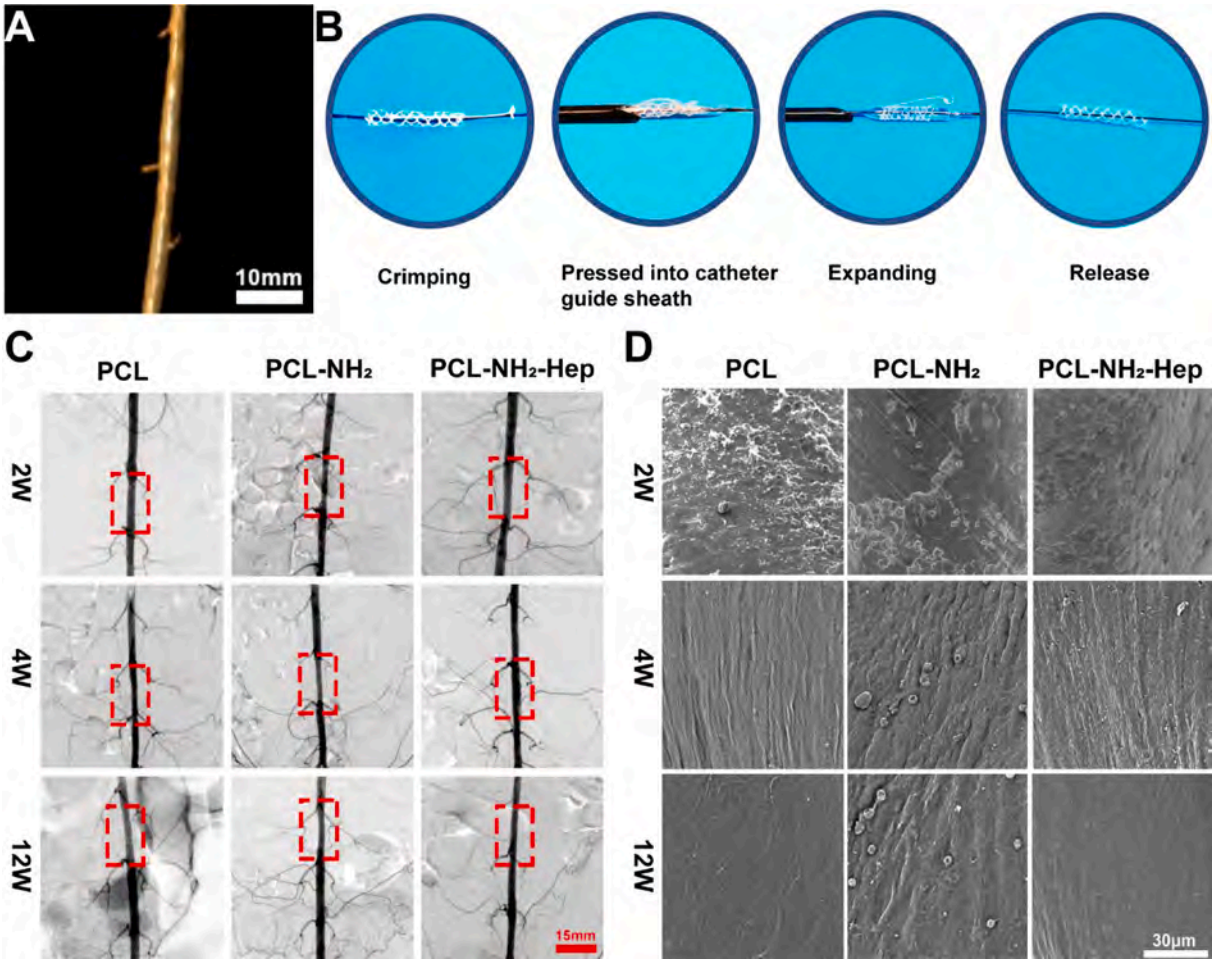

Fig. 8. (A) Representative MRA images of rabbit abdominal aorta used for *in vivo* study. (B) Digital photos of 3D printed stent-balloon delivery system. (C) Representative angiography images of PCL, PCL-NH_2 and PCL-NH_2-Hep stent implanted vessels after 2 weeks, 4 weeks and 12 weeks implantations. (D) SEM micrographs of endothelialization of the inner surface of the stents after PCL, PCL-NH_2 and PCL-NH_2-Hep stents were implanted for 2 weeks, 4 weeks and 12 weeks.

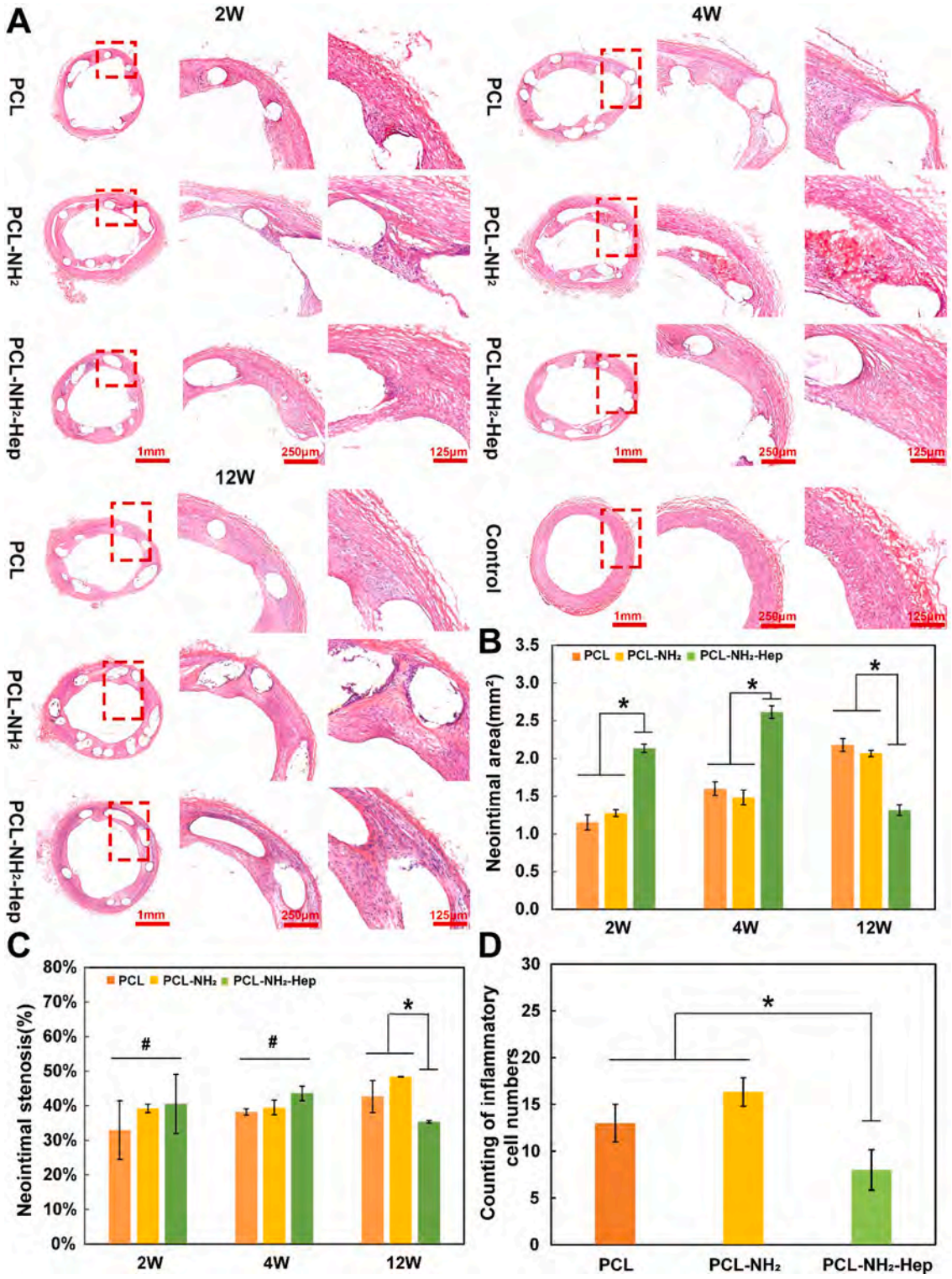

Fig. 9. (A) H&E staining images of PCL, PCL-NH_2 and PCL-NH_2-Hep stent implanted vessels during 12 weeks follow-up. (B) Neointimal areas of stented vessels during 12 weeks follow-up, measured from H&E staining images. (C) Neointimal stenosis of stented vessels during 12 weeks follow-up, measured from H&E staining images. (D) Inflammatory cell numbers in the neointima during 12 weeks follow-up (*Indicates significant difference of $p < 0.05$. # Indicates no significant difference of $p > 0.05$).

gradually integrated with the stent. The stented vessels showed great patency. While no significant thrombosis was found around the PCL and PCL-NH_2-Hep stent within 12 weeks of implantation. Thrombus formation could be observed around the PCL-NH_2 stent. This result was consistent with the angiography images. After stents implantation, neointima gradually formed to heal the injured blood vessel wall. We observed that the average neointimal area of PCL-NH_2-Hep stent was larger than that of PCL and PCL-NH_2 in 2 weeks and 4 weeks. However, the average neointimal area (Fig. 9B) of PCL-NH_2-Hep stent (1.31 mm^2) decreased significantly compared with PCL group (2.18 mm^2) and PCL-NH_2 group (2.07 mm^2) at 12 weeks. Meanwhile, the neointimal stenosis rate (Fig. 9C) of heparinized stents (35.36 %) was significantly lower

than that of PCL (40.6 %) and PCL-NH_2 (43.6 %). Therefore, the introduction of heparin may reduce the incidence of in-stent restenosis by inhibiting neointimal hyperplasia. Moreover, the inflammatory cell numbers in the neointima in the PCL-NH_2-Hep group was lower than that of PCL and PCL-NH_2 group at 12 weeks (Fig. 9D).

Immunohistochemical fluorescence (Fig. 10A) and immunohistochemical staining (Fig. 10B) showed that CD31 (a typical marker of ECs) was positive and concentrated in the outer layer of neointima around PCL-NH_2-Hep stent, which proved that relatively complete endothelialization was produced. While some endothelial cells were gathered around the PCL and PCL-NH_2 stents, but no continuous endothelium was formed. α-SMA (a typical marker of SMCs) also indicated the orderly remodeling of vascular tissue around the PCL-NH_2-Hep stent. CD68(a typical marker of macrophages) showed that no obvious immune response was observed in the neointima around PCL-NH_2-Hep stent after 3 months implantation.

4. Discussion

As the incidence of coronary artery disease increase continually, the need for cardiovascular stents as an important treatment method is increasing. In clinical application, the latest generation of drug-eluting stent has become an effective tool for percutaneous intervention[34]. But it fails to address the limitations of permanent metal coronary stent, such as inflammation, intimal hyperplasia and neoarteriosclerosis[35]. And the risk of extremely late stent restenosis remains exist. Biodegradable polymer is a promising stent material for blood vessels because of its biodegradability[36]. Biodegradable stents are able to support diseased arteries to restore normal blood flow and finally be degraded to avoid permanent retention.

At present, braiding technique and laser engraving can be applied to the preparation of biodegradable stents. But they all have the limitations, such as low radial force of braided stents and the thermal damage on laser-cutting stent. Stent size may also not match the size of the diseased vessel, resulting in failure of implantation or restenosis of the vessel. 3D printing is a widely concerned technology in recent years. It can be customized according to the patient's specific diseased vessels, and then applied to the precise repair and treatment of blood vessels. Circular strut of 3D printed stent can reduce the interference of blood flow, which is more beneficial for endothelialization. At present, there is insufficient study about 3D printed stent implantation in rabbit arteries. In the work, we designed the model based on the MRA imaging data of animal blood vessel, and fabricated the PCL stent via 3D printing, followed by covalent grafting with heparin to improve their anticoagulant ability. Then we employed a 3D printed stent-balloon delivery system to deliver 3D printed stents to the rabbit abdominal aorta, and evaluated the feasibility of implantation (Fig. 8B).

PCL has been used in the preparation of vascular grafts and other cardiovascular devices due to its satisfactory biocompatibility and biodegradability[37]. However, PCL tend to form thrombus on the surface of the material due to lack of anticoagulant properties and antiplatelet ability[38,39]. The surface of PCL does not contain activated groups, so it is necessary to realize surface activation by grafting functional groups on the surface of the polyester. In order to introduce amino groups, PCL stents were treated with 1,6-hexanediamine, which provided activated sites for heparinization. The –NH_2 groups, which on the surface of stents, were demonstrated by Ninhydrin hydrate staining. Then heparin can react with –NH_2 groups on the surface of PCL-NH_2 to obtain PCL-NH_2-Hep stent. This approach took advantage of amino groups on the surface of PCL-NH_2 and allowed the introduction of polysaccharide molecule heparin. By toluidine blue staining, the presence of assembled heparin can be also verified. SEM images showed that amination and heparinization had no significant effect on the morphology and structure of stents.

It is well known that intravascular thrombosis is one of the main problems after coronary stent implantation. Platelets adhere and aggregate on the surface of the injured intima, leading to the formation of thrombus. The anticoagulation and platelet adhesion of PCL, PCL-NH_2 and PCL-NH_2-Hep stents were evaluated. We found that grafting Heparin onto the surface of the aminated PCL effectively reduced the ability of platelets adhesion and inhibited platelet activation (Fig. 6B). The main mechanism can be the interaction of heparin with Antithrombin III (ATIII), which promotes ATIII-mediated inhibition of thrombin and coagulation factor XA[40]. Moreover, the enhancement of the surface hydrophilicity of stents may maintain the normal protein conformation and prevent the activation of platelets. The results of PT and APTT test were entirely coincided with the SEM figures of platelet adhesion. DSA also showed that the blood vessels showed great patency after PCL-NH_2-Hep stent implantation (Fig. 8C). These results showed that heparin molecules have excellent anticoagulant properties, which is consistent

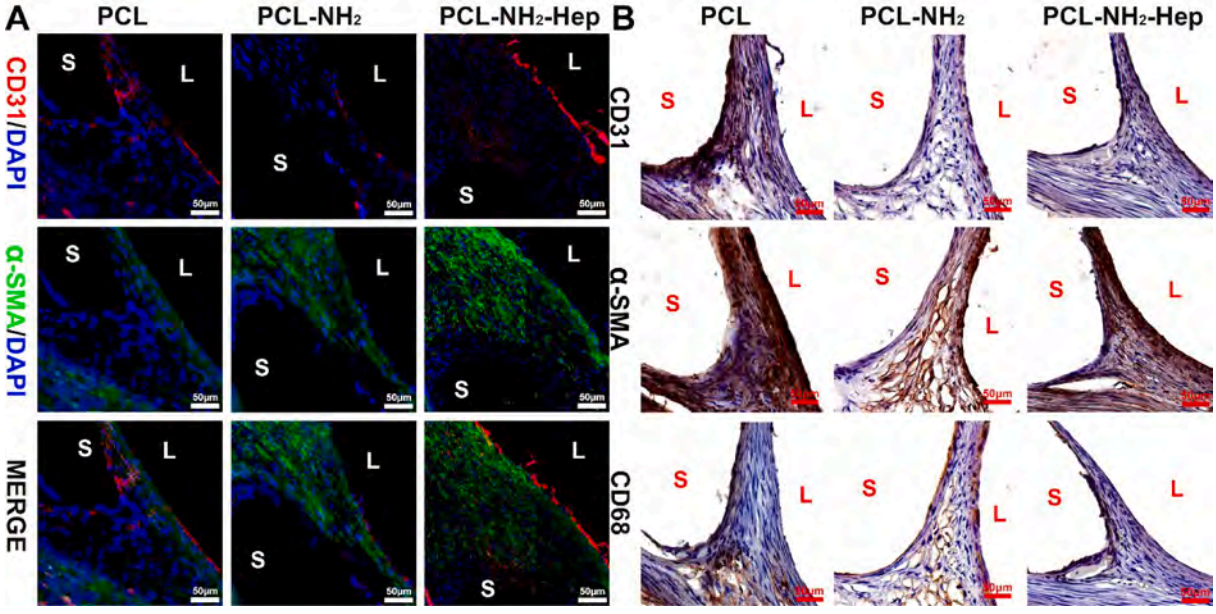

Fig. 10. (A) Immunofluorescence staining of the stented arterial enface for CD31, α-SMA and DAPI during 12 weeks follow-up. (B) Immunohistochemical staining of the stented arterial enface for CD31, α-SMA and CD68 during 12 weeks follow-up. vessel lumen is marked as 'L', cross section of stents is marked as 'S'.

with previous reports[41,42]. For PCL stents, slight stenosis was observed in stented vessel. Compared with PCL and PCL-NH_2-Hep stents, obvious stenosis occurred in PCL-NH_2 group after stent implantation. which was consistent with the results of platelet adhesion *in vitro*. The PCL-NH_2 stents showed more platelet adhesion. Large amounts of amino groups on the surface reacted with biomolecules on the platelet membrane surface to promote platelet adhesion and activation. Moreover, previous studies have reported that the interaction between platelet and inflammatory cells could mediate thrombo-inflammation. The activated platelets released multiple substances: α-granules, δ-granules, and lysosomes, which could influence on inflammation [43]. We found that the inflammatory cell numbers in the neointima in the PCL-NH_2-Hep group was lower than that of PCL and PCL-NH_2 group (Fig. 9D). We speculate that the introduction of heparin could inhibit the platelet activation so that reduce inflammatory response.

Intimal hyperplasia and positive vascular remodeling occur simultaneously during stent implantation[44–46]. During this period, the interaction between ECs and SMCs plays an important role in the recovery of vascular function and morphology. In the process of vascular remodeling, neointima gradually forms to heal the injured blood vessel wall. ECs can sense the changes of vascular environment, which is very important in the process of vascular remodeling[47]. Heparin is essential for promoting ECs adhesion and proliferation. We observed that HUVECs had higher cell coverage and better adhesion and proliferation on heparin-modified stents than PCL stents (Fig. 7A, B). Liu et al. reported that Heparin could not only effectively inhibit the adhesion and activation of platelets, but also promote the proliferation of endothelial progenitor cells and endothelial cells[48]. Covalently grafted heparin molecules provide an identifiable biological site for endothelial cells, thus facilitating adhesion of HUVECs to the stent. Moreover, the interaction between heparin and vascular growth factor can also improve cell adhesion. We also found that neointima area increased within 1 month after PCL-NH_2-Hep stent implantation. The average neointima area in the PCL-NH_2-Hep group was larger than that of PCL and PCL-NH_2 group (Fig. 9B). We speculate that the effective repair of vascular endothelium at the initial stage of stent implantation promotes vascular remodeling and regeneration with the help of heparin.

In the process of vascular remodeling, the disorders of SMCs migration, proliferation and secretion of constitute the basic pathological characteristics of intimal hyperplasia[33,49]. Heparin has shown the potential to inhibit the excessive proliferation of SMCs by preventing the cell cycle from entering the G1 phase by reducing the activation of extracellular signal-regulated kinases[50]. The presence of heparin transforms the SMCs from a synthetic phenotype to a contractile phenotype. We observed that SMCs on heparin-modified stents had lower cell coverage than PCL stents, and that cell adhesion and proliferation were also inhibited (Fig. 7D, E). The introduction of heparin regulated proliferation of SMCs to prevent intimal hyperplasia and in-stent restenosis. At the same time, we found that PCL and PCL-NH_2 stent showed persistent intimal hyperplasia after 3 months implantation. However, the neointimal area and neointimal stenosis rate of PCL-NH_2-Hep stents decreased significantly at 3 months (Fig. 9B, C). This may be closely related to the introduction of heparin. The recovery of endothelial layer function, the inhibition of SMCs excessive proliferation and vascular remodeling may effectively reduce the incidence of vascular restenosis.

In this study, we focus on the evaluation of the implantation of the PCL, PCL-NH_2 and PCL-NH_2-Hep stent within 12 weeks. According to our results, PCL-NH_2-Hep stent can promote the adhesion, spreading and proliferation of ECs cells without stenosis and occlusion. It is worth noting that the current research has some limitations. We have implanted 3D printed stents into the abdominal aorta of rabbits, but the application in living animal models of atherosclerosis is obviously a better evaluation model. Meanwhile, we realize that the stent implantation period is so short that we cannot observe significant material degradation of the graft. PCL may degrade within 2–3 years after implantation. Therefore, our future research will focus on the long-term results of PCL-NH_2-Hep stents in large animal models.

5. Conclusion

Based on 3D printing and surface modification, a personalized biodegradable stent with anticoagulant function was successfully developed, and the possibility of implantation in rabbit abdominal aorta was evaluated. The results showed that the 3D printed stents had strong compressive properties and good flexibility. Surface modification of heparin could improve the hydrophilicity of PCL-NH_2-Hep stent, reducing the adhesion of platelets. It could also promote the adhesion and proliferation of ECs, and inhibit the proliferation of SMCs. The possibility of implanting in rabbit abdominal aorta was evaluated. The stent showed good biocompatibility and mechanical strength within 12 weeks and maintained patency without acute thrombosis formation in an implantation of the rabbit abdominal artery. These results confirmed the potential of 3D printing personalized, anticoagulant, and biodegradable coronary artery stents guided by MRA for vascular repair.

Ethics statement

All animal experiments were conducted according to the medical guidelines of Shanghai Jiao Tong University School for the housing and care of laboratory animals (Animal welfare and ethics acceptance No. 2020-0524) and performed following institutional regulations after pertinent review and approval by Shanghai Jiao Tong University School of Medicine on Animal Care.

Declaration of Competing Interest

The authors declare that they have no known competing financial interests or personal relationships that could have appeared to influence the work reported in this paper.

Data availability

No data was used for the research described in the article.

Acknowledgements

This work was supported by National Natural Science Foundation of China (No. 81501606, No. 32050410286, No. 81771951), Science and Technology Commission of Shanghai Municipality (No. 20S31900900, 20DZ2254900), Sino German Science Foundation Research Exchange Center (M-0263), Shanghai Pujiang Program (2020PJD043), Shanghai Science and Technology Innovation Project (201409006000). This work was also supported by Researchers Supporting Project Number (RSP-2021/65), King Saud University, Riyadh, Saudi Arabia, National Advanced Functional Fiber Innovation Center (2021-fx020301).

References

[1] G. Roth, G. Mensah, C. Johnson, G. Addolorato, E. Ammirati, L. Baddour, N. Barengo, A. Beaton, E. Benjamin, C. Benziger, A. Bonny, M. Brauer, M. Brodmann, T. Cahill, J. Carapetis, A. Catapano, S. Chugh, L. Cooper, J. Coresh, M. Criqui, N. DeCleene, K. Eagle, S. Emmons-Bell, V. Feigin, J. Fernández-Solà, G. Fowkes, E. Gakidou, S. Grundy, F. He, G. Howard, F. Hu, L. Inker, G. Karthikeyan, N. Kassebaum, W. Koroshetz, C. Lavie, D. Lloyd-Jones, H. Lu, A. Mirijello, A. Temesgen, A. Mokdad, A. Moran, P. Muntner, J. Narula, B. Neal, M. Ntsekhe, G. Moraes de Oliveira, C. Otto, M. Owolabi, M. Pratt, S. Rajagopalan, M. Reitsma, A. Ribeiro, N. Rigotti, A. Rodgers, C. Sable, S. Shakil, K. Sliwa-Hahnle, B. Stark, J. Sundström, P. Timpel, I. Tleyjeh, M. Valgimigli, T. Vos, P. Whelton, M. Yacoub, L. Zuhlke, C. Murray, V. Fuster, Global Burden of Cardiovascular Diseases and Risk Factors, 1990-2019: Update From the GBD 2019 Study, J. Am. Coll. Cardiol. 76(25) (2020) 2982-3021. https://doi.org/10.1016/j.jacc.2020.11.010.

[2] G. Heusch, B. Gersh, The pathophysiology of acute myocardial infarction and strategies of protection beyond reperfusion: a continual challenge, Eur. Heart J. 38 (11) (2017) 774–784, https://doi.org/10.1093/eurheartj/ehw224.

[3] A.A. Oliver, M. Sikora-Jasinska, A.G. Demir, R.J. Guillory 2nd, Recent advances and directions in the development of bioresorbable metallic cardiovascular stents: Insights from recent human and in vivo studies, Acta Biomater. 127 (2021) 1–23, https://doi.org/10.1016/j.actbio.2021.03.058.

[4] S. Garg, C. Bourantas, P. Serruys, New concepts in the design of drug-eluting coronary stents, Nat Rev Cardiol 10 (5) (2013) 248–260, https://doi.org/10.1038/nrcardio.2013.13.

[5] H. Jinnouchi, S. Torii, A. Sakamoto, F.D. Kolodgie, R. Virmani, A.V. Finn, Fully bioresorbable vascular scaffolds: lessons learned and future directions, Nat Rev Cardiol 16 (5) (2019) 286–304, https://doi.org/10.1038/s41569-018-0124-7.

[6] I. Cockerill, C.W. See, M.L. Young, Y. Wang, D. Zhu, Designing better cardiovascular stent materials: A learning curve, Adv. Funct. Mater. 31 (1) (2021) 2005361, https://doi.org/10.1002/adfm.202005361.

[7] J. Wiebe, H. Nef, C. Hamm, Current status of bioresorbable scaffolds in the treatment of coronary artery disease, J. Am. Coll. Cardiol. 64 (23) (2014) 2541–2551, https://doi.org/10.1016/j.jacc.2014.09.041.

[8] T. Hu, C. Yang, S. Lin, Q. Yu, G. Wang, Biodegradable stents for coronary artery disease treatment: Recent advances and future perspectives, Mater. Sci. Eng. C Mater. Biol. Appl. 91 (2018) 163–178, https://doi.org/10.1016/j.msec.2018.04.100.

[9] H.Y. Ang, H. Bulluck, P. Wong, S.S. Venkatraman, Y. Huang, N. Foin, Bioresorbable stents: Current and upcoming bioresorbable technologies, Int. J. Cardiol. 228 (2017) 931–939, https://doi.org/10.1016/j.ijcard.2016.11.258.

[10] F. Zhao, J. Sun, W. Xue, F. Wang, M.W. King, C. Yu, Y. Jiao, K. Sun, L. Wang, Development of a polycaprolactone/poly(p-dioxanone) bioresorbable stent with mechanically self-reinforced structure for congenital heart disease treatment, Bioact Mater 6 (9) (2021) 2969–2982, https://doi.org/10.1016/j.bioactmat.2021.02.017.

[11] N. Azzi, W. Shatila, Update on coronary artery bioresorbable vascular scaffolds in percutaneous coronary revascularization, Rev. Cardiovasc. Med. 22 (1) (2021) 137–145. https://doi.org/10.31083/j.rcm.2021.01.225.

[12] B. Polanec, J. Kramberger, S. Glodez, A review of production technologies and materials for manufacturing of cardiovascular stents, Adv Prod Eng Manag 15 (4) (2020) 390–402. https://doi.org/10.14743/apem2020.4.373.

[13] T. Zou, L. Wang, W. Li, W. Wang, F. Chen, M.W. King, A resorbable bicomponent braided ureteral stent with improved mechanical performance, J. Mech. Behav. Biomed. Mater. 38 (2014) 17–25, https://doi.org/10.1016/j.jmbbm.2014.06.004.

[14] A.G. Demir, B. Previtali, C.A. Biffi, fibre laser cutting and chemical etching of AZ31 for manufacturing biodegradable stents, Adv Mater Sci Eng 2013 (2013) 1–11, https://doi.org/10.1155/2013/692635.

[15] H. Jia, S.-Y. Gu, K. Chang, 3D printed self-expandable vascular stents from biodegradable shape memory polymer, Adv. Polym. Tech. 37 (8) (2018) 3222–3228, https://doi.org/10.1002/adv.22091.

[16] S.K. Misra, F. Ostadhossein, R. Babu, J. Kus, D. Tankasala, A. Sutrisno, K.A. Walsh, C.R. Bromfield, D. Pan, 3D-printed multidrug-eluting stent from graphene-nanoplatelet-doped biodegradable polymer composite, Adv Healthc Mater 6 (11) (2017), https://doi.org/10.1002/adhm.201700008.

[17] S.J. Lee, H.H. Jo, K.S. Lim, D. Lim, S. Lee, J.H. Lee, W.D. Kim, M.H. Jeong, J.Y. Lim, I.K. Kwon, Y. Jung, J.-K. Park, S.A. Park, Heparin coating on 3D printed poly (l-lactic acid) biodegradable cardiovascular stent via mild surface modification approach for coronary artery implantation, Chem. Eng. J. 378 (2019), https://doi.org/10.1016/j.cej.2019.122116.

[18] J.M. Jiménez, P.F. Davies, Hemodynamically driven stent strut design, Ann. Biomed. Eng. 37 (8) (2009) 1483–1494, https://doi.org/10.1007/s10439-009-9719-9.

[19] S. Im, Y. Jung, S. Kim, Current status and future direction of biodegradable metallic and polymeric vascular scaffolds for next-generation stents, Acta Biomater. 60 (2017) 3–22, https://doi.org/10.1016/j.actbio.2017.07.019.

[20] M.A. Woodruff, D.W. Hutmacher, The return of a forgotten polymer—Polycaprolactone in the 21st century, Prog. Polym. Sci. 35 (10) (2010) 1217–1256, https://doi.org/10.1016/j.progpolymsci.2010.04.002.

[21] P.S. Damus, M. Hicks, R.D. Rosenberg, Anticoagulant action of heparin, Nature 246 (5432) (1973) 355–357, https://doi.org/10.1038/246355a0.

[22] T. Zhu, H. Gu, H. Zhang, H. Wang, H. Xia, X. Mo, J. Wu, Covalent grafting of PEG and heparin improves biological performance of electrospun vascular grafts for carotid artery replacement, Acta Biomater. 119 (2021) 211–224, https://doi.org/10.1016/j.actbio.2020.11.013.

[23] J. Zhu, D. Chen, J. Du, X. Chen, J. Wang, H. Zhang, S. Chen, J. Wu, T. Zhu, X. Mo, Mechanical matching nanofibrous vascular scaffold with effective anticoagulation for vascular tissue engineering, Compos Part B-Eng 186 (2020), https://doi.org/10.1016/j.compositesb.2020.107788.

[24] D. Lei, B. Luo, Y. Guo, D. Wang, H. Yang, S. Wang, H. Xuan, A. Shen, Y. Zhang, Z. Liu, C. He, F.-L. Qing, Y. Xu, G. Zhou, Z. You, 4-Axis printing microfibrous tubular scaffold and tracheal cartilage application, Sci China Mater 62 (12) (2019) 1910–1920, https://doi.org/10.1007/s40843-019-9498-5.

[25] C. Li, J. Mao, Q. Li, F. Wang, Y. Jiao, Z. Zhang, R. Guidoin, L. Wang, Long-term anticoagulation and selective cells adhesion surface via combination of covalent grafting and layer by layer assembly, Biomed. Mater. 14 (6) (2019), 065012, https://doi.org/10.1088/1748-605X/ab452b.

[26] X. Xie, D. Li, Y. Chen, Y. Shen, F. Yu, W. Wang, Z. Yuan, Y. Morsi, J. Wu, X. Mo, Conjugate electrospun 3D gelatin nanofiber sponge for rapid hemostasis, Adv Healthc Mater 10 (20) (2021) e2100918.

[27] Y. Zhu, Z. Mao, C. Gao, Aminolysis-based surface modification of polyesters for biomedical applications, RSC Adv 3 (8) (2013) 2509–2519, https://doi.org/10.1039/C2RA22358A.

[28] Y. Zhu, C. Gao, X. Liu, J. Shen, Surface modification of polycaprolactone membrane via aminolysis and biomacromolecule immobilization for promoting cytocompatibility of human endothelial cells, Biomacromolecules 3 (6) (2002) 1312–1319, https://doi.org/10.1021/bm020074y.

[29] F.J. Beerkens, B.E. Claessen, M. Mahan, M.F.L. Gaudino, D.Y. Tam, J.P. S. Henriques, R. Mehran, G.D. Dangas, Contemporary coronary artery bypass graft surgery and subsequent percutaneous revascularization, Nat Rev Cardiol (2021), https://doi.org/10.1038/s41569-021-00612-6.

[30] U.T. Seyfert, V. Biehl, J. Schenk, In vitro hemocompatibility testing of biomaterials according to the ISO 10993–4, Biomol. Eng. 19 (2–6) (2002) 91–96, https://doi.org/10.1016/s1389-0344(02)00015-1.

[31] K. Stang, S. Krajewski, B. Neumann, J. Kurz, M. Post, S. Stoppelkamp, S. Fennrich, M. Avci-Adali, D. Armbruster, C. Schlensak, Hemocompatibility testing according to ISO 10993–4: Discrimination between pyrogen-and device-induced hemostatic activation, Mater Sci Eng C 42 (2014) 422–428, https://doi.org/10.1016/j.msec.2014.05.070.

[32] D. Bassir, L. Yang, X. Chen, L. Zhang, L. Li, S. Kang, C. Wang, W. Sun, Additive manufacturing in vascular stent fabrication, MATEC Web of Conferences 253 (2019), https://doi.org/10.1051/matecconf/201925303003.

[33] A.C. Newby, A.B. Zaltsman, Molecular mechanisms in intimal hyperplasia, J Pathol 190 (3) (2000) 300–309, https://doi.org/10.1002/(SICI)1096-9896(200002)190:3<300::AID-PATH596>3.0.CO;2-I.

[34] S. Torii, H. Jinnouchi, A. Sakamoto, M. Kutyna, A. Cornelissen, S. Kuntz, L. Guo, H. Mori, E. Harari, K. Paek, R. Fernandez, D. Chahal, M. Romero, F. Kolodgie, A. Gupta, R. Virmani, A. Finn, Drug-eluting coronary stents: insights from preclinical and pathology studies, Nature reviews. Cardiology 17 (1) (2020) 37–51, https://doi.org/10.1038/s41569-019-0234-x.

[35] T. Hu, J. Yang, K. Cui, Q. Rao, T. Yin, L. Tan, Y. Zhang, Z. Li, G. Wang, Controlled slow-release drug-eluting stents for the prevention of coronary restenosis: recent progress and future prospects, ACS Appl Mater Interfaces 7 (22) (2015) 11695–11712, https://doi.org/10.1021/acsami.5b01993.

[36] S. McMahon, N. Bertollo, E.D.O. Cearbhaill, J. Salber, L. Pierucci, P. Duffy, T. Dürig, V. Bi, W. Wang, Bio-resorbable polymer stents: a review of material progress and prospects, Prog. Polym. Sci. 83 (2018) 79–96, https://doi.org/10.1016/j.progpolymsci.2018.05.002.

[37] B.W. Tillman, S.K. Yazdani, S.J. Lee, R.L. Geary, A. Atala, J.J. Yoo, The in vivo stability of electrospun polycaprolactone-collagen scaffolds in vascular reconstruction, Biomaterials 30 (4) (2009) 583–588, https://doi.org/10.1016/j.biomaterials.2008.10.006.

[38] A.F. Martins, S.P. Facchi, P.C. da Câmara, S.E. Camargo, C.H. Camargo, K.C. Popat, M.J. Kipper, Novel poly (ε-caprolactone)/amino-functionalized tannin electrospun membranes as scaffolds for tissue engineering, J. Colloid Interface Sci. 525 (2018) 21–30, https://doi.org/10.1016/j.jcis.2018.04.060.

[39] O. Suwantong, Biomedical applications of electrospun polycaprolactone fiber mats, Polym. Adv. Technol. 27 (10) (2016) 1264–1273, https://doi.org/10.1002/pat.3876.

[40] E. Marciniak, J. Gockerman, Heparin-induced decrease in circulating antithrombin-III, The Lancet 310 (8038) (1977) 581–584, https://doi.org/10.1016/s0140-6736(77)91429-5.

[41] A. Yin, R. Luo, J. Li, X. Mo, Y. Wang, X. Zhang, Coaxial electrospinning multicomponent functional controlled-release vascular graft: Optimization of graft properties, Colloids Surf. B. Biointerfaces 152 (2017) 432–439, https://doi.org/10.1016/j.colsurfb.2017.01.045.

[42] H. Kuang, Y. Wang, J. Hu, C. Wang, S. Lu, X. Mo, A method for preparation of an internal layer of artificial vascular graft co-modified with salvianolic acid b and heparin, ACS Appl Mater Interfaces 10 (23) (2018) 19365–19372, https://doi.org/10.1021/acsami.8b02602.

[43] P.E.J. van der Meijden, J.W.M. Heemskerk, Platelet biology and functions: new concepts and clinical perspectives, Nat Rev Cardiol 16 (3) (2019) 166–179, https://doi.org/10.1038/s41569-018-0110-0.

[44] L.A. Guzman, M.J. Mick, A.M. Arnold, F. Forudi, P.L. Whitlow, Role of intimal hyperplasia and arterial remodeling after balloon angioplasty: an experimental study in the atherosclerotic rabbit model, Arterioscler. Thromb. Vasc. Biol. 16 (3) (1996) 479–487, https://doi.org/10.1161/01.atv.16.3.479.

[45] G.H. Gibbons, V.J. Dzau, The emerging concept of vascular remodeling, N. Engl. J. Med. 330 (20) (1994) 1431–1438, https://doi.org/10.1056/NEJM199405193302008.

[46] C. Indolfi, S. De Rosa, A. Colombo, Bioresorbable vascular scaffolds — basic concepts and clinical outcome, Nat Rev Cardiol 13 (12) (2016) 719–729, https://doi.org/10.1038/nrcardio.2016.151.

[47] D.B. Cowan, B.L. Langille, Cellular and molecular biology of vascular remodeling, Curr. Opin. Lipidol. 7 (2) (1996) 94–100, https://doi.org/10.1097/00041433-199604000-00008.

[48] Y. Liu, R. Luo, F. Shen, L. Tang, J. Wang, N. Huang, Construction of mussel-inspired coating via the direct reaction of catechol and polyethyleneimine for efficient heparin immobilization, Appl. Surf. Sci. 328 (2015) 163–169, https://doi.org/10.1016/j.apsusc.2014.12.004.

[49] M.W. Liu, G. Roubin, S. King 3rd, Restenosis after coronary angioplasty Potential biologic determinants and role of intimal hyperplasia, Circulation 79 (6) (1989) 1374–1387, https://doi.org/10.1161/01.cir.79.6.1374.

[50] M. Ottlinger, L.A. Pukac, M.J. Karnovsky, Heparin inhibits mitogen-activated protein kinase activation in intact rat vascular smooth muscle cells, J. Biol. Chem. 268 (26) (1993) 19173–19176, https://doi.org/10.1016/S0021-9258(19)36492-0.